Journal of Bacteriology

Bacteriology | Full-Length Text

Involvement of ArlI, ArlJ, and CirA in archaeal type IV pilin-mediated motility regulation

Priyanka Chatterjee,[1,2] Marco A. Garcia,[1] Jacob A. Cote,[1,2] Kun Yun,[1] Georgio P. Legerme,[1] Rumi Habib,[2,3] Manuela Tripepi,[1] Criston Young,[1] Daniel Kulp,[2,3] Mike Dyall-Smith,[4,5] Mecky Pohlschroder[1]

AUTHOR AFFILIATIONS See affiliation list on p. 16.

ABSTRACT Many prokaryotes use swimming motility to move toward favorable conditions and escape adverse surroundings. Regulatory mechanisms governing bacterial flagella-driven motility are well-established; however, little is yet known about the regulation underlying swimming motility propelled by the archaeal cell surface structure, the archaella. Previous research showed that the deletion of the adhesion pilins (PilA1-6), subunits of the type IV pili cell surface structure, renders the model archaeon *Haloferax volcanii* non-motile. In this study, we used ethyl methanesulfonate mutagenesis and a motility assay to identify motile suppressors of the Δ*pilA*[*1-6*] strain. Of the eight suppressors identified, six contain missense mutations in archaella biosynthesis genes, *arlI* and *arlJ*. *In trans* expression of *arlI* and *arlJ* mutant constructs in the respective multi-deletion strains Δ*pilA*[*1-6*]Δ*arlI* and Δ*pilA*[*1-6*]Δ*arlJ* confirmed their role in suppressing the Δ*pilA*[*1-6*] motility defect. Additionally, three suppressors harbor co-occurring disruptive missense and nonsense mutations in *cirA*, a gene encoding a proposed regulatory protein. A deletion of *cirA* resulted in hypermotility, while *cirA* expression *in trans* in wild-type cells led to decreased motility. Moreover, quantitative real-time PCR analysis revealed that in wild-type cells, higher expression levels of *arlI*, *arlJ*, and the archaellin gene *arlA1* were observed in motile early-log phase rod-shaped cells compared to non-motile mid-log phase disk-shaped cells. Conversely, Δ*cirA* cells, which form rods during both early- and mid-log phases, exhibited similar expression levels of *arl* genes in both growth phases. Our findings contribute to a deeper understanding of the mechanisms governing archaeal motility, highlighting the involvement of ArlI, ArlJ, and CirA in pilin-mediated motility regulation.

IMPORTANCE Archaea are close relatives of eukaryotes and play crucial ecological roles. Certain behaviors, such as swimming motility, are thought to be important for archaeal environmental adaptation. Archaella, the archaeal motility appendages, are evolutionarily distinct from bacterial flagella, and the regulatory mechanisms driving archaeal motility are largely unknown. Previous research has linked the loss of type IV pili subunits to archaeal motility suppression. This study reveals three *Haloferax volcanii* proteins involved in pilin-mediated motility regulation, offering a deeper understanding of motility regulation in this understudied domain while also paving the way for uncovering novel mechanisms that govern archaeal motility. Understanding archaeal cellular processes will help elucidate the ecological roles of archaea as well as the evolution of these processes across domains.

KEYWORDS archaea, archaella, motility regulation, type IV pili, cell shape, swimming motility, *Haloferax*, circadian

Microorganisms have evolved sophisticated motility machineries that allow them to adeptly navigate their diverse environments, for example, to acquire nutrients or

Editor Julie A. Maupin-Furlow, Department of Microbiology and Cell Science, University of Florida, Gainesville, Florida, USA

Address correspondence to Mecky Pohlschroder, pohlschr@sas.upenn.edu.

The authors declare no conflict of interest.

See the funding table on p. 16.

Received 5 March 2024
Accepted 6 May 2024
Published 31 May 2024

to avoid toxins (1, 2). In Bacteria, the rotation of flagella promotes swimming motility. However, in Archaea, evolutionarily distinct rotating surface filaments called archaella drive swimming motility (3–5). The biosynthesis machinery of archaella is evolutionarily related to that of type IV pili (T4P), which are appendages required for bacterial and archaeal surface motility, as well as adhesive interactions required for biofilm formation (6–10). For instance, the subunits of both structures—archaellins in archaella and pilins in T4P—share class III signal peptides, which are required for transport to the cell surface and are processed by homologous signal peptidases (8). Moreover, key assembly proteins, such as ArlI and ArlJ for archaella, and PilB and PilC for T4P, also exhibit remarkable homology, suggesting a deeper evolutionary connection between these seemingly disparate cell surface structures.

The archaellin genes are often found in a gene cluster (11–13) along with genes encoding components of the archaellum motor complex, such as the ATPase ArlI, which assembles into the hexameric rotor, and the membrane protein anchor ArlJ (11, 13). The components of the archaellum motor also include the ATP-binding protein ArlH (14) and stator proteins ArlF and ArlG (15, 16). In Euryarchaeota [Methanobacteriota (17)], ArlC/D/E, or any combination or fusion of the three, are thought to serve as a scaffold for the motor (7, 18). In Crenarchaeota [Thermoproteota (19)], a putative membrane protein ArlX is thought to replace ArlC/D/E (13, 15).

Recent studies have elucidated the regulatory roles of proteins encoded by genes in the *arl* cluster of some archaea. Both the euryarchaeal *Pyrococcus furiosus* and the crenarchaeal *Sulfolobus acidocaldarius* ArlH homologs have been shown to autophosphorylate. In the non-phosphorylated state, ArlH hexamerizes and associates with the ArlI rotor, but upon phosphorylation of ArlH, its affinity for ArlI is reduced. Deleting *arlH* or abrogating the phosphorylation of ArlH results in a loss of cell motility, signifying an important regulatory role for ArlH (14, 20, 21). While little is known about other aspects of archaella regulation, many euryarchaeal ArlH homologs contain a KaiC domain. KaiC family ATPases, which are named after a key component of the circadian clock proteins of cyanobacteria, have been proposed to have signal transduction roles in archaea (22).

The motility phenotype of the euryarchaeon, *Haloferax volcanii*, correlates with its cell shape. Transitions between motile rod-shaped cells and sessile disk-shaped cells can be observed in liquid culture (23) or in motility halos formed after cells are stab-inoculated into soft agar (24). Cells observed in the early-log growth phase or at the edge of the motility halos are motile, rod-shaped, and exhibit archaella on their surface. In the mid-to-late log growth phase or at the center of the motility halos, they present as sessile, non-archaellated, pleomorphic disks (23, 24). Reported mutants that cannot form rods are unable to swim (24, 25). Conversely, mutants that are locked in the rod shape tend to be hypermotile (25).

In our previous study, two mutants isolated from a hypermotility screen were rod-only in the conditions tested. Those mutants had premature stop codons in the gene *cirA,* which encodes Circadian regulator CirA (25). Similar to ArlH, CirA is also a KaiC-like protein, and *cirA* is located within the *arl* gene cluster (22). Like the cyanobacterial circadian clock proteins, transcription of *cirA* oscillates with a light/dark cycle (26). Thus, the positioning of *cirA* proximal to the *arl* genes, along with the proposed importance of KaiC-like proteins in archaeal signal transduction (22), suggests that CirA may play a role in motility regulation.

Esquivel *et al*. reported that the conserved hydrophobic domain (H-domain) of type IV pilins is not only required for adhesion but is also involved in motility regulation (27). This N-terminal H-domain is critical for the assembly of pilins into a pilus fiber (6) and is also part of the class III signal peptide. This signal peptide contains a unique signal peptidase cleavage site N-terminal to the H-domain (28). Upon cleavage, processed pilins are incorporated into a pilus. It has been proposed that a subset of processed pilins is retained in the membranes of planktonic cells. Esquivel *et al*. found that deleting all six *H. volcanii* adhesion pilins containing this conserved H-domain (Δ*pilA*[*1-6*]) results in a loss of both adhesion and swimming motility. Expression *in trans* of the H-domain

fused to a non-pilin protein is unable to restore surface adhesion but can restore motility in these cells (27). This suggests that, in addition to increasing surface adhesion, the assembly of these pilins into pili may also promote biofilm formation by preventing membrane-associated pilins from enabling archaella-driven motility. The mechanism by which the depletion of pilins inhibits motility is not well understood.

Here, we describe a motility screen that identified suppressor mutants of the non-motile Δ*pilA*[*1-6*]. Most of the suppressors harbor missense point mutations in *arlI* and/or *arlJ*. Using reverse genetics, we have demonstrated that these mutations enable cells to swim despite lacking the pilin H-domains. Additionally, a subset of these suppressors harbors disruptive mutations in *cirA*. Transcriptional analysis of a Δ*cirA* strain suggests that CirA reduces expression of the *arl* genes, revealing a novel avenue of motility regulation.

RESULTS

Ethyl methanesulfonate mutagenesis of Δ*pilA*[*1-6*] revealed motile suppressors

To identify components involved in H-domain-dependent motility regulation, we began by screening for suppressors of the motility defect of the Δ*pilA*[*1-6*] mutant strain. Since spontaneous motile mutants of Δ*pilA*[*1-6*] streaked across a soft-agar motility plate were not identified after incubation for 5 days, we screened with chemically induced mutations. Cells were incubated with 0.05 M ethyl methanesulfonate (EMS) for 0, 10, 20, and 30 minutes. The 20-minute incubation was the shortest exposure time that resulted in suppressors that could form motility halos (Fig. 1). After streaking cells from the edge of the motility halo onto solid agar plates, isolated colonies were picked and stabbed onto soft agar motility plates to confirm the motility phenotype. Eight suppressors of the Δ*pilA*[*1-6*] motility defect were isolated using this method.

The majority of Δ*pilA*[*1-6*] suppressor mutants contain mutations in *arlI, arlJ*, and/or *cirA*

To identify the genes altered by EMS mutagenesis, genomic DNA isolated from the eight suppressor mutants was sent for whole-genome sequencing (WGS; Table S1). All of the suppressor strains had multiple mutations. The total number of mutations ranged between 7 and 35, not including the engineered deletion of PilA[1-6]. Most mutations occur in only one suppressor strain. Only three genes (*arlI*, *arlJ*, and *cirA*) were identified as having distinct mutations in at least two Δ*pilA*[*1-6*] suppressor strains (Table 1; Table S1), suggesting the significance of these genes in the suppressor phenotype. Moreover, *arlI*, *arlJ*, and *cirA* are all located in the same genomic region, strongly suggesting a link to pilin-mediated motility regulation. While multiple mutants encoding ArlI^{A331V} and ArlJ^{A364V} were identified, these strains have different secondary mutations (Table S1) and total number of mutations (Table 1). Moreover, strains with the same mutation were isolated from different plates, indicating that the mutations occurred independently, strongly suggesting that the mutations in these specific residues play a role in the suppression of the motility defect of Δ*pilA*[*1-6*]. Two suppressors, KY-7 and KY-8, have mutations in both *arlI* and *cirA*, and one suppressor, KY-1, includes mutations in all three genes (Table 1). This suggests that the proteins encoded by these genes may work in combination to regulate motility: co-occurrence of two unrelated mutations in two genes of one gene cluster is much less probable than a single occurrence; therefore, co-occurrence of two mutations might indicate that the single mutations alone are not enough to induce the phenotype. ArlJ^{A364V} does not co-occur with mutations in either ArlI or CirA, which may indicate a significant role of this residue in motility regulation.

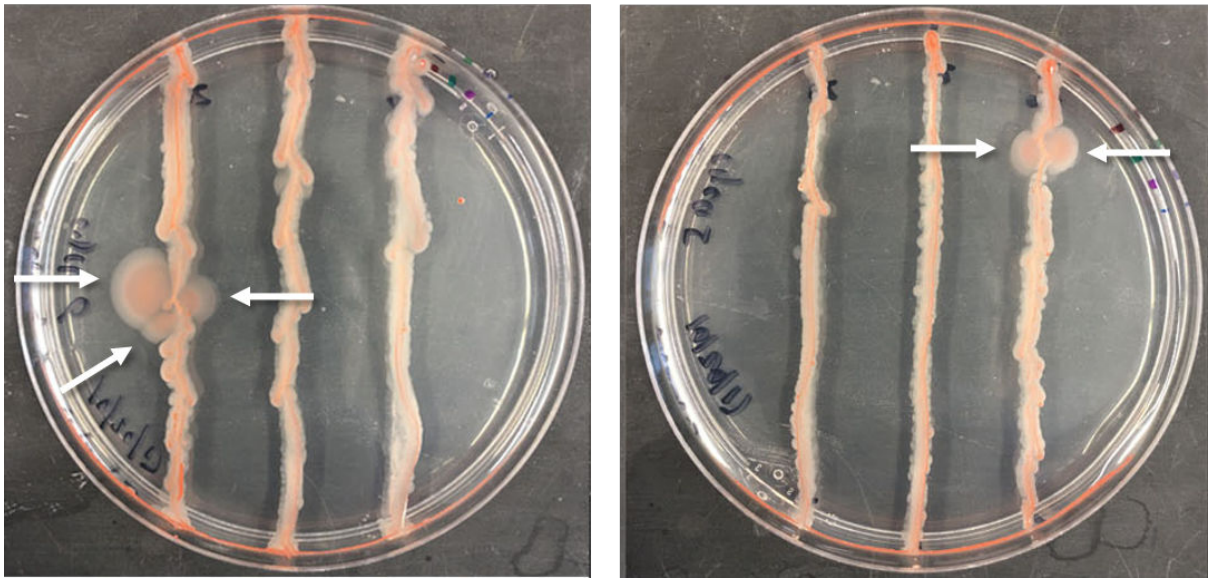

FIG 1 EMS mutagenesis results in Δ*pilA*[*1-6*] suppressor mutants that regain swimming motility. Two representative images of soft agar plates [0.3% (wt/vol)] that have been streaked with *H. volcanii* Δ*pilA*[*1-6*] incubated with 0.05 M EMS for 20 minutes. White arrows point to motility halos of suppressors after 5 days of incubation at 45°C.

Δ*pilA*[*1-6*] suppressors have mutations that may slightly alter the functions of ArlI and ArlJ but disrupt CirA

In the Δ*pilA*[*1-6*] motile suppressors, most of the amino acid substitutions in ArlI and ArlJ retain the same chemical properties as the replaced residue, such as in the alanine or glycine substitutions for valine in ArlI^{A331V} and ArlJ^{A364V}, which retain aliphaticity, and the tyrosine substitution for phenylalanine in ArlJ^{Y358F}, which retains aromaticity. ArlI^{D356H} is the only mutation in ArlI and ArlJ that results in a major change in the properties of the residue: aspartate changed to histidine (Table 1). To assess whether the mutated residues affect conserved regions of the proteins, we aligned the *H. volcanii* ArlI and ArlJ protein sequences with those of four haloarchaeal homologs, as well as five homologs from representative archaeal species of different phyla (Fig. 2A and B; Fig. S1).

Mapping the two ArlI residues mutated in the suppressor mutants (Table 1), we found that the residue at position 331 of ArlI occurs just prior to the Aspartate Box, which is involved in divalent cation binding (29). While ArlI A331 is not highly conserved across the species included in our alignment, the residues that align with *H. volcanii* A331 are generally aliphatic (Fig. 2A). The replacement mutation ArlI^{A331V} was identified in two separately isolated suppressors, KY-1 and KY-8 (Table 1), suggesting the importance of alanine with regard to suppression of the Δ*pilA*[*1-6*] motility phenotype. *H. volcanii* ArlI D356 is in a region with one or two negatively charged amino acids (Fig. 2A).

TABLE 1 Δ*pilA*[*1-6*] motility suppressors

Strain name	ArlI mutation	ArlJ mutation	CirA mutation	Total mutations[c]
KY-1	A331V	Y358F	G19S	7
KY-3	–[a]	A364V	–	13
KY-4	–	A364V	–	10
KY-5	–	A364V	–	23
KY-7	D356H	–	W199*[b]	16
KY-8	A331V	–	G33E	35

[a]–, no mutation; wild-type sequence.
[b]*, stop codon.
[c]Total mutations refer to mutations in addition to those engineered in the Δ*pilA*[*1-6*] strain.

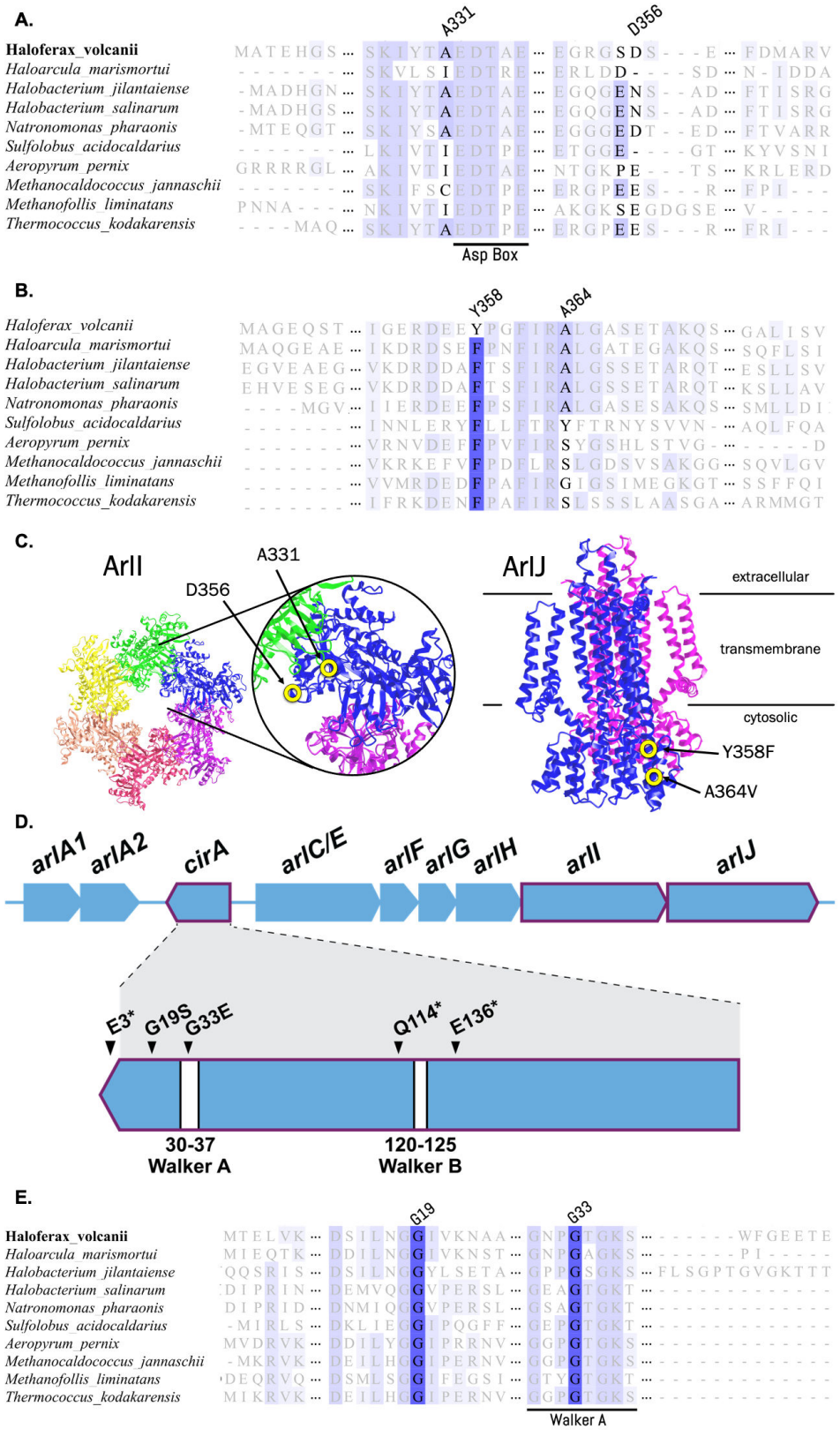

FIG 2 Residues of interest as sequence alignments, 3D structures, and genomic locations. Sequence alignments of (A) ArlI, (B) ArlJ, and (E) CirA from *H. volcanii* with homologs from four additional haloarchaeal species and five non-halophilic archaeal species of different phyla. Regions of the alignment surrounding the mutated residues from Table 1 are shown; other regions

(Continued on next page)

FIG 2 (Continued)

of the protein are either omitted or set to 25% transparency to ease visualization. Conserved residues across species are indicated in shades of blue, with darker blues corresponding to highly conserved residues. The ArlI conserved Aspartate Box motif and the CirA Walker A domain are indicated. (C) Residues of ArlI and ArlJ corresponding to Δ*pilA*[*1-6*] suppressor mutations mapped to the AlphaFold structure predictions of the ArlI hexamer and ArlJ dimer, respectively. Yellow circles indicate the residues of interest. (D) *cirA* is found between the archaellin genes (*arlA1* and *arlA2*) and the rest of the *arl* genes (*arlC/E–arlJ*). It is transcribed in the opposite direction as the *arl* genes. The genic locations of the residues corresponding to the mutations found in the Δ*pilA*[*1-6*] suppressor mutants as well as hypermotile mutants from a previous study (25) are indicated, along with the conserved Walker A and Walker B motifs.

Similarly, we mapped the single residue changes of ArlJ from the suppressor mutants in the protein sequence alignments for this membrane protein. The residue at position 358 in *H. volcanii* ArlJ, which is mutagenized from tyrosine to a phenylalanine residue in the suppressor strain KY-1 (Table 1), is a phenylalanine residue in all of the other species used in our alignment (Fig. 2B). The alanine at position 364 of ArlJ is conserved in the haloarchaeal sequences aligned.

To determine the location of these mutations on the three-dimensional proteins, we generated AlphaFold structural predictions (30) of the wild-type *H. volcanii* ArlI hexamer and ArlJ dimer (Fig. 2C). The locations of the residues at position 331 and 356 on the ArlI structure suggest that they are potentially part of interaction sites with ArlJ or other interacting partners. Additionally, the *H. volcanii* ArlI^{D356} residue overlaps with the corresponding residue E312 from the published structure of *S. acidocaldarius* FlaI (ArlI) (31) (Fig. S2a). For ArlJ, consistent with a potential interaction with cytoplasmic ArlI, the mutated residues appear not to affect the dimer interface and map to the cytoplasmic region as determined by SignalP 6.0 (32) (Fig. 2C).

Although *cirA* is found in the same genomic region as *arlI* and *arlJ*, it is transcribed in the reverse direction (Fig. 2D), and in contrast to the *arlI* and *arlJ* suppressors, the *cirA* suppressors harbor disruptive missense or nonsense mutations. One of these mutations results in a premature stop codon (CirA^{W199*}), while the other two substitutions result in significant changes in the chemical properties (CirA^{G19S} and CirA^{G33E}; Table 1). Protein sequence alignment of *H. volcanii* CirA with the homologs of the same species used for ArlI and ArlJ revealed that G19 and G33 are highly conserved across species (Fig. 2E). The mutation for CirA^{G33E} appears within the conserved Walker A ATPase motif present in the KaiC-like domain (Fig. 2D). The premature stop codon and other disruptive mutations in *cirA* strongly support the idea that suppression of the Δ*pilA*[*1-6*] motility defect requires inactivation of CirA.

The ArlI and ArlJ mutations suppress the Δ*pilA*[*1-6*] motility defect and retain the archaella biogenesis function

To confirm that the mutated residues in ArlI and ArlJ contribute to the suppression of the Δ*pilA*[*1-6*] motility defect, we constructed Δ*arlI* and Δ*arlJ* strains as well as Δ*pilA*[*1-6*] strains also lacking either *arlI* or *arlJ*. The wild-type *arlI* and *arlJ* genes as well as *arlI* and *arlJ* genes with mutations corresponding to the suppressor mutants (Table 1) were inserted into the expression vector pTA963 (33). Each construct was transformed into the corresponding single deletion strain of Δ*arlI* or Δ*arlJ* as well as into the multi-deletion strains Δ*pilA*[*1-6*]Δ*arlI* or Δ*pilA*[*1-6*]Δ*arlJ*.

The Δ*arlI* and Δ*arlJ* strains are non-motile, but stab-inoculates of these strains overexpressing wild-type ArlI and ArlJ, respectively, on soft agar result in motility halos. The expression *in trans* of ArlI^{A331V} or ArlI^{D356H} from an overexpression vector pTA963 in the Δ*arlI* background also supports motility on soft agar, although the motility halo for the deletion strain expressing ArlI^{D356H} is smaller than that of ArlI or ArlI^{A331V} (Fig. 3). This supports the view that these mutations do not deactivate the archaella biosynthesis function of ArlI. Similarly, the expression *in trans* of either ArlJ^{Y358F} or ArlJ^{A364V} complements the Δ*arlJ* motility defect. In fact, *in trans* expression of the point mutations

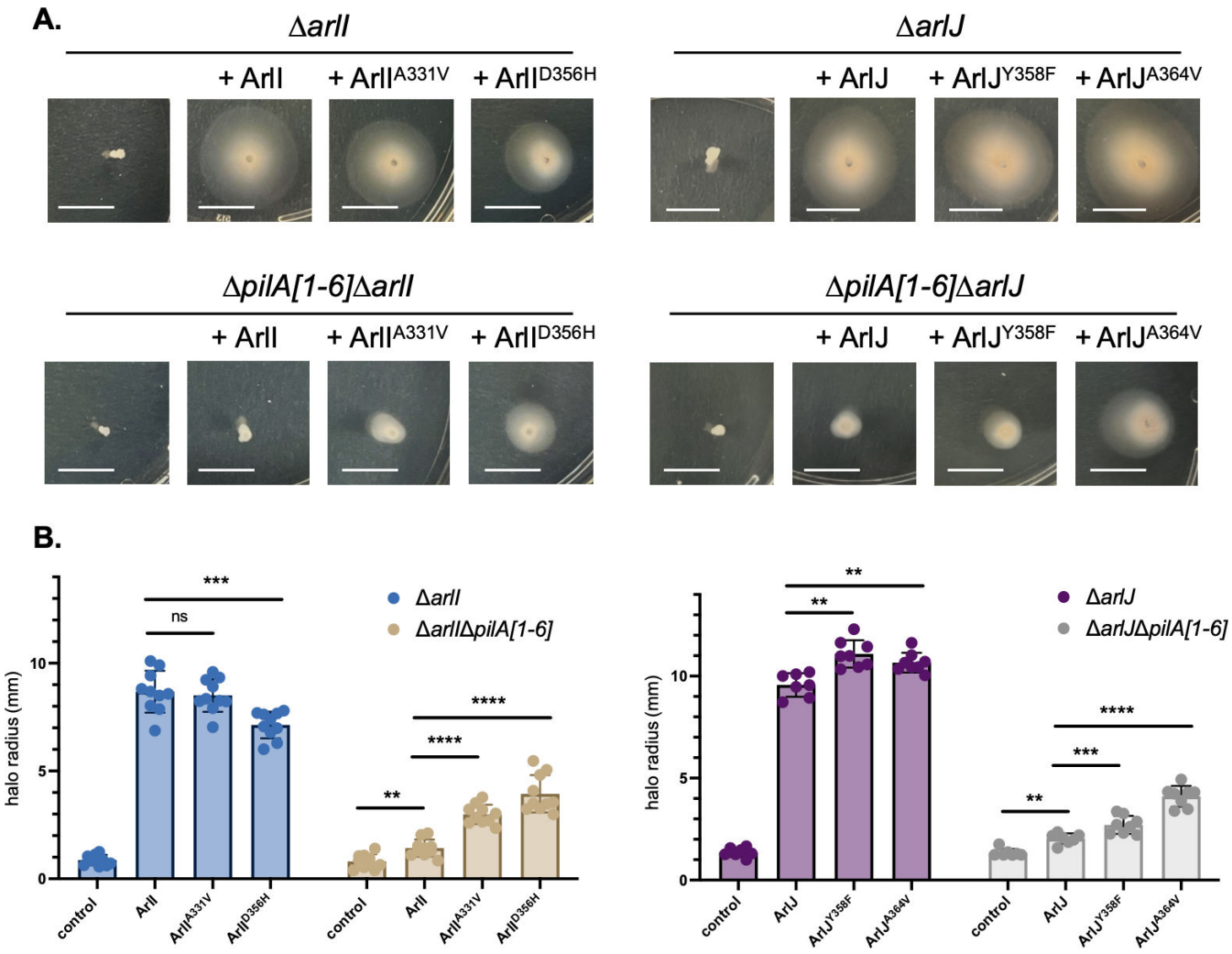

FIG 3 Overexpression of mutant ArlI or ArlJ results in differential motility. (A) pTA963 expression vectors containing genes encoding either wild-type or mutant proteins were transformed into the indicated deletion strains. Empty vector was also transformed as control for all four deletion strains. Cells were stab-inoculated into 0.3% (wt/vol) agar plates, incubated at 45°C for 3 days, and then at room temperature for 1 day before imaging. White bar represents 1 cm. (B) Quantification of halo radius in millimeters across 7–10 replicates for each strain. Statistical analysis was performed using the unpaired nonparametric *t* test. $^{**}P < 0.01$, $^{***}P < 0.001$, and $^{****}P < 0.0001$.

results in slightly larger motility halos as compared to that of ArlJ, indicating that these mutations also do not interfere with archaella biogenesis.

Δ*pilA*[*1-6*]Δ*arlI* and Δ*pilA*[*1-6*]Δ*arlJ* are, as expected, non-motile. Expression *in trans* of ArlI and ArlJ in the respective multi-deletion strains results in minimal motility, possibly due to the high abundance of plasmid-encoded ArlI or ArlJ, respectively. Supporting the importance of the point mutations, ArlI^{A331V} and ArlI^{D356H} expressions result in significantly increased motility than the expression of the wild-type copy. The Δ*pilA*[*1-6*]Δ*arlI* strain expressing ArlI^{D356H} *in trans* has a larger motility halo than the strain expressing ArlI^{A331V}, suggesting that the D356H mutation is more effective for overcoming the loss of pilins. Similarly, the expression of ArlJ^{Y358F} and ArlJ^{A364V} in Δ*pilA*[*1-6*]Δ*arlJ* results in notable increases in the motility halo radius when compared to the expression of ArlJ in this strain. Additionally, ArlJ^{A364V} results in a larger motility halo than ArlJ^{Y358F}, implying that it is more effective at suppressing the phenotype (Fig. 3). These results indicate that the single residue mutations in ArlI and ArlJ can enable motility in the absence of the conserved H-domain of the pilins.

CirA suppresses swimming motility

Expression of ArlI or ArlJ in the multi-deletion strains led to a statistically significant increase in the motility halo radius compared to the negative control containing only the overexpression vector (Fig. 3), suggesting that increasing the abundance of ArlI or ArlJ can partially overcome pilin-mediated motility suppression. Since (i) CirA is predicted to have regulatory roles (22), (ii) *cirA* is found adjacent to the archaella genes (Fig. 2D), and (iii) three of the Δ*pilA*[*1-6*] motile suppressors have CirA disruptions along with missense mutations in ArlI and/or ArlJ (Table 1), we hypothesized that CirA regulates motility by affecting the abundance of ArlI and ArlJ.

To study the effects of disrupting CirA function, we generated the deletion strain Δ*cirA*. While Δ*cirA* is hypermotile, complementation with *cirA* expressed from pTA963 reverses this effect and significantly reduces the size of Δ*cirA* motility halos. Furthermore, the expression *in trans* of CirA in wild-type *H. volcanii* results in reduced motility (Fig. 4), suggesting that CirA plays a role in repressing motility.

Deletion of *cirA* results in smaller colonies, disk-deficiency, and decreased light scattering

Since KaiC-like ATPases are hypothesized to be major hubs of complex regulatory networks in archaea (22), it follows that CirA could serve several regulatory roles in *H. volcanii*. Consistent with this idea, the loss of CirA results in several phenotypic changes in this haloarchaeon. Δ*cirA*, compared to wild type, forms smaller, darker colonies when streaked on an Hv-Cab solid agar plate (Fig. S3a) and also produces a smaller, darker cell pellet upon centrifugation of mid-log phase cultures, grown to OD_{600} 0.55 (Fig. S3b). Using a plate reader equipped to monitor OD_{600} values, Δ*cirA*, after entering the exponential phase, lagged by about 3 hours, equivalent to approximately one doubling time, compared to the wild type (Fig. S3c). Additionally, since Δ*cirA* is hypermotile (Fig. 4), and motility is often associated with the rod shape (24), we investigated Δ*cirA* cell shape. Interestingly, Δ*cirA* does not transition to disk-shaped cells at the mid-log growth phase like the wild type and remains as rod-shaped (Fig. 5). Considering the shape difference as well as the pellet size difference between Δ*cirA* and wild type, we wanted to determine

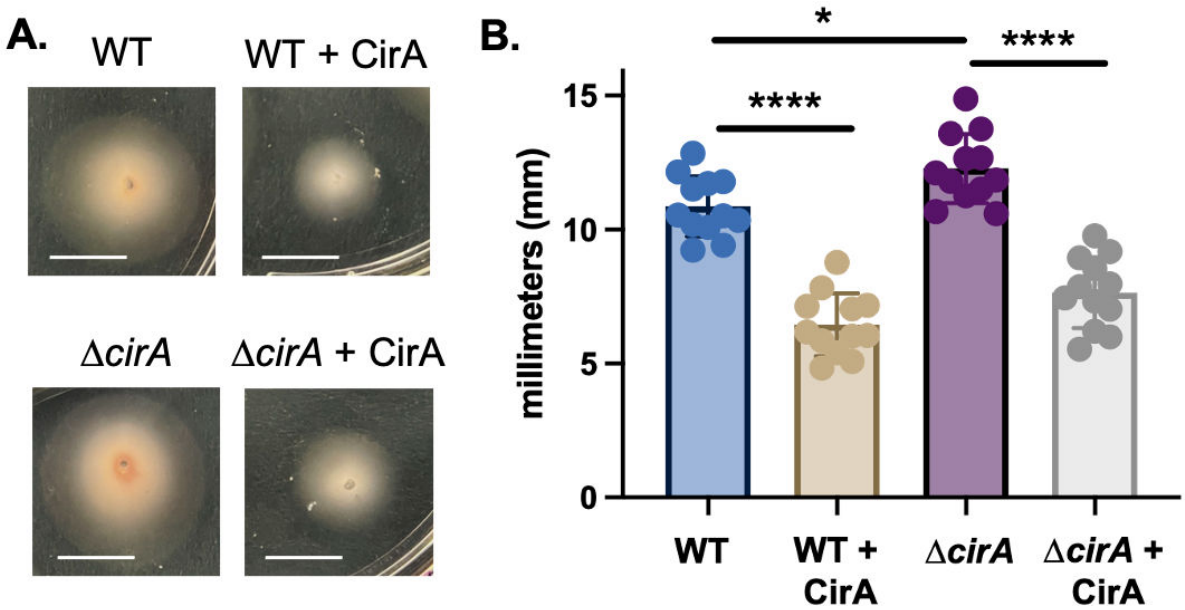

FIG 4 Overexpression of CirA results in reduced motility. (A) Empty pTA963 or vector containing *cirA* was transformed into wild-type and Δ*cirA* strains. Cells were stab-inoculated onto 0.3% (wt/vol) agar plates, incubated at 45°C for 3 days, then at room temperature for 1 day before imaging. White bar represents 1 cm. (B) Quantification of halo radius across 12 replicates of each stabbed strain. Statistical analysis was performed using the unpaired nonparametric *t* test. *P < 0.05 and ****P < 0.0001.

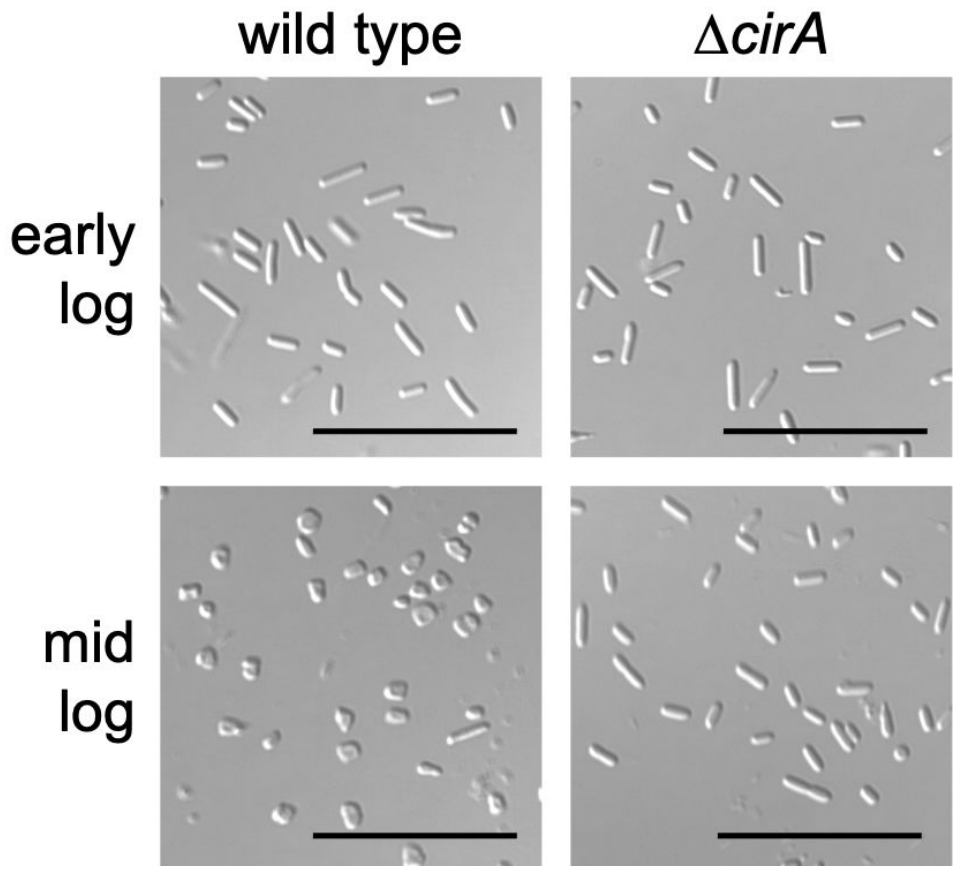

FIG 5 Δ*cirA* remains rod-shaped in the mid-log phase. Early-log (OD_{600} 0.05) and mid-log (OD_{600} 0.35) phase cultures of wild-type and Δ*cirA* were harvested, and cells were imaged using differential interference contrast (DIC). The black bar represents 20 µm.

whether the cell count of these cultures at the same OD_{600} is comparable. Surprisingly, colony-forming units (CFU) counts of cultures grown to OD_{600} 0.5 yielded nearly four times the number of cells in Δ*cirA* compared to wild type (Fig. S3d), indicating that using optical density to measure *H. volcanii* cell growth may not always accurately reflect doubling time.

CirA regulates motility by reducing the transcription of *arl* genes

Since expression *in trans* of CirA results in reduced motility (Fig. 4), compounded with our observations that Δ*cirA* is hypermotile (Fig. 4) and has a prolonged rod stage (Fig. 5), we predicted that the loss of CirA affects the abundance of archaellins and the archaella biosynthetic components. Quantitative real-time PCR (qRT-PCR) studies, indeed, revealed that as wild-type cells begin the transition from rod-shaped in early-log to disk-shaped in mid-log, the transcription of genes encoding the archaellin (ArlA1) and archaella biosynthetic components (ArlI and ArlJ) decreases (Fig. 6). Transcription levels of all three genes are higher in Δ*cirA* early-log when compared to wild-type early-log, and the higher levels are maintained as Δ*cirA* transitions into mid-log. Thus, *cirA* plays a role in the transcription of the *arl* genes.

DISCUSSION

It has been proposed that during biofilm formation, *H. volcanii* rapidly assembles membrane-sequestered pilins into type IV pili in order to promote surface adhesion. Thus, the pilins are depleted from the membrane, which leads to the cessation of motility

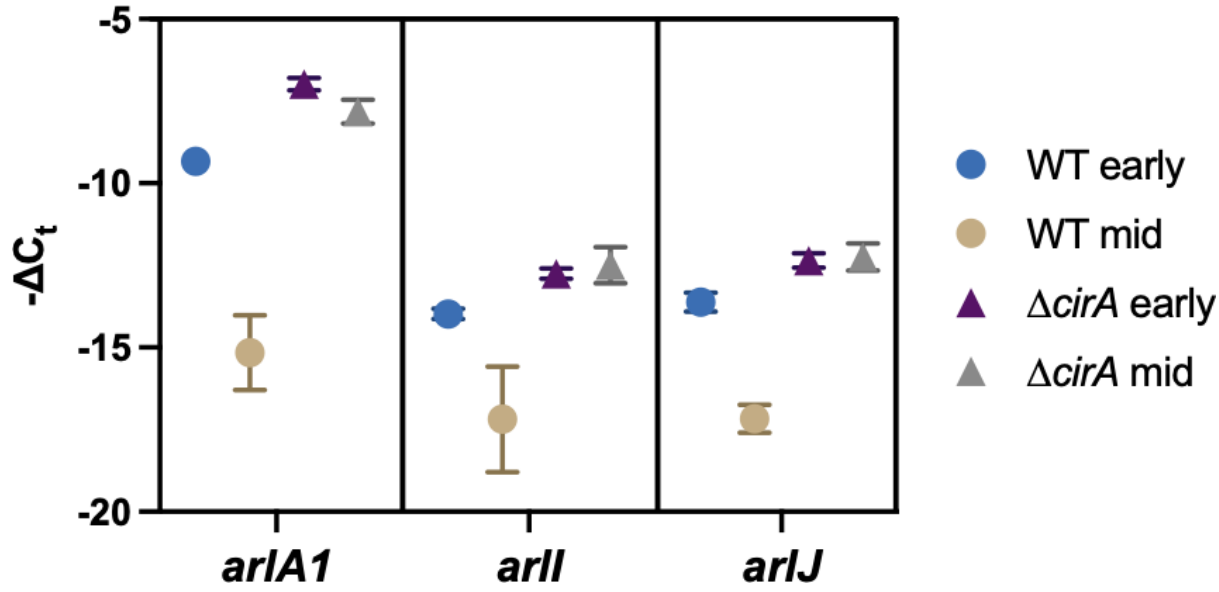

FIG 6 Δ*cirA* displays a different transcription profile of *arlA1*, *arlI*, and *arlJ* than wild type. qRT-PCR was conducted using primers for 16S rRNA, *arlA1*, *arlI*, and *arlJ* under the following conditions: (i) wild type at early-log; (ii) wild type at mid-log; (iii) Δ*cirA* at early-log; and (iv) Δ*cirA* at mid-log. Values are shown as the negative difference in threshold crossing point $-\Delta C_t$ of *arlA1*, *arlI*, and *arlJ* relative to 16S rRNA. Error bars represent the SD of five technical replicates.

(27). This loss of motility due to a depletion of membrane-sequestered pilins is presumably mimicked by the Δ*pilA*[*1-6*] strain. In this study of the mutations that arose in motile suppressors of the Δ*pilA*[*1-6*] strain, we have discovered a novel aspect of *H. volcanii* motility regulation. The identification of several suppressor mutations in genes encoding ArlI and ArlJ suggested that by altering specific residues in these archaella biosynthetic components, motility can be restored to the non-motile Δ*pilA*[*1-6*] strain. Indeed, we revealed with reverse genetics that the mutated proteins, which can complement the respective *arlI* and *arlJ* deletion strains, can partially restore motility to the multi-deletion strains Δ*pilA*[*1-6*]Δ*arlI* and Δ*pilA*[*1-6*]Δ*arlJ* (Fig. 3A). It is interesting to note that while the deletion of the pilin genes is a major inhibitor of motility, partial restoration of motility can still provide insights into this biological process.

Most of the suppressor mutations are point mutations in *arlI* and *arlJ* that result in single residue changes that retain the same chemical properties as the replaced residue. Therefore, it is possible that these slight variations of key residues alter the binding affinity(s) of these proteins to other proteins. Alignments of ArlI reveal that the D356 residue aligns with a region that contains one or two negatively charged amino acids in the other homologs, including an aspartate in *S. acidocaldarius* that forms a putative salt bridge between subunits of the hexamer (31). In *H. volcanii* ArlI, D356 may form a salt bridge with H234 (Fig. S2B), an interaction that seems to be disrupted in ArlI^{D356H}. The disruption of this putative salt bridge may explain the reduced motility of the *in trans* expression of ArlI^{D356H} compared to that of ArlI and ArlI^{A331V} in the Δ*arlI* strain (Fig. 3). The increased motility of the *in trans* expression of ArlI^{D356H} in Δ*pilA*[*1-6*]Δ*arlI* may still be due to the mutation altering binding affinity to partner proteins. Mutations in ArlJ do not suggest their involvement in dimer production, but their cytoplasmic location may indicate interactions with cytoplasmic proteins, such as ArlI, suggesting that binding affinity for a partner protein at the cytoplasmic interface is altered. In the case that the point mutations in ArlI and ArlJ lead to increased binding affinity, the interactions between binding partners that are necessary for motility could be increased, and thus, the mutants are able to synthesize archaella despite missing the conserved pilin H-domain. Conversely, if the point mutations lead to decreased binding, it is possible that the mutant proteins no longer bind to inhibitory proteins that suppress motility and become capable of swimming without the H-domain. Additional explanations for

these phenotypes exist, for example, that the point mutations alter the half-life of the protein and thereby increase the intracellular concentration. Thus, further analysis of the interactome of ArlI and ArlJ through protein-protein interaction studies may not only elucidate additional components involved in pilin-mediated motility regulation but also provide insights into the effects of the point mutations.

In the motile suppressors of Δ*pilA*[*1-6*], mutations in *cirA* arose concurrently with several mutations in the archaella biosynthetic components (Table 1). A potential link between CirA and hypermotility has been alluded to in a previous study, where an *H. volcanii* transposon mutant (JK3) had been identified as hypermotile. While the gene disrupted by the transposon did not lead to hypermotility, the WGS of the transposon mutants uncovered a secondary mutation in *cirA* (25). The secondary mutation resulted in a premature stop codon at the third amino acid (CirA^{E3*}). Similarly, in the Δ*pilA*[*1-6*] suppressors, the *cirA* mutation in KY-7 results in a premature stop codon, and the KY-1 and KY-8 strains harbor disruptive *cirA* point mutations in highly conserved residues (Fig. 2E). Here, we show that a Δ*cirA* strain is indeed hypermotile, potentially due to the lack of CirA-dependent *arl* gene regulation.

In our previous study, we discovered, using quantitative proteomics, that the archaellin ArlA1 has a significantly lower abundance in the late-log phase than the early-log phase, while CirA increases in abundance across the growth phases (25). Interestingly, ArlA1 abundance is not as drastically different in the growth phase comparisons of JK3, suggesting that CirA is involved in the regulation of ArlA1. While differences in protein abundance of ArlI or ArlJ were not observed in wild type or JK3(25), the abundance of archaella biosynthetic components could be below the detection level of a quantitative proteomics experiment, consistent with the absence of any ArlI or ArlJ peptides identified in the Archaeal Proteome Project database (34). However, a study in another halophilic species found that while protein abundance changes for the archaella biosynthetic proteins in the tested experimental conditions were not found, transcriptional analysis was able to identify differences in the regulation of *arl* genes (35). Furthermore, another study reported that sessile, disk-shaped biofilm-derived cells can exhibit a decreased expression of *arl* genes (36). Corroborating those findings, in this study, we detected decreases in the transcription levels of not only *arlA1* but also of *arlI* and *arlJ*, between early-log phase rods and mid-log phase disks in wild type. This decrease was not observed in the Δ*cirA* strain (Fig. 6), supporting our hypothesis that CirA is involved in the downregulation of *arlA1*, *arlI*, and *arlJ*. These findings begin to elucidate the role of CirA on the transcriptional regulation of certain *arl* genes, and further transcriptomics or RNA-seq studies on Δ*cirA* will continue to delineate the effects on other genes in the *arl* operon as well as potential additional genes.

It is yet unknown whether CirA functions directly as a regulator of the transcription or indirectly as an intermediary in a regulatory network. CirA is transcribed in the opposite direction as the *arl* genes (Fig. 2D), but it is unlikely that the act of transcribing CirA reduces the transcription of the *arl* genes because the expression of CirA from the pTA963 plasmid also reduces motility (Fig. 4). It is also important to note that the loss of CirA affects more than just motility, including the inability to form disks in the conditions tested (Fig. 5) and the formation of smaller colonies (Fig. S3A). Additionally, pellets of Δ*cirA* cells in liquid cultures grown to the same OD_{600} as wild type are also smaller even though viability counts reveal strikingly higher cell numbers (Fig. S3b and d), suggesting that CirA affects the overall density of the cells, potentially by modulating cell surface composition. Interestingly, the OD_{600} growth curve did reveal that both wild type and Δ*cirA* cells reach a similar optical density at the stationary phase (Fig. S3C). While more in-depth studies of cell culture growth of wild type and Δ*cirA* are needed, the multiple physiological differences between these two strains observed in this study support that CirA is a broad regulatory protein in *H. volcanii*. Expression of *cirA* has been shown to oscillate in a light-/dark-dependent manner, reminiscent of the KaiC regulator. In fact, one of the suppressor mutations, CirA^{G33E}, occurs within the Walker A motif, a region that has previously been shown to induce an arrhythmic phenotype when

mutated (37). Further characterization of CirA function will elucidate the mechanism by which it suppresses motility, affects physiology, and potentially modulates *H. volcanii* light-dependent behavior.

Lastly, additional mutations in the Δ*pilA*[*1-6*] suppressor mutants may also play a role in motility regulation. In particular, KY-2 and KY-6 lack mutations in *arlI*, *arlJ*, or *cirA* (Table S1). Repeating our motility screen could help narrow down additional important components to further help elucidate mechanisms of motility regulation in *H. volcanii*.

In conclusion, in this study, we used the model organism *H. volcanii* to uncover that ArlI and ArlJ are involved in pilin-mediated motility regulation and identified critical residues important to this regulatory function. Furthermore, we have determined a novel role for CirA in motility regulation and revealed its importance in disk formation and cell density.

MATERIALS AND METHODS

Growth conditions

The plasmids and strains used in this study are listed in Tables S2 and S3. *H. volcanii* H53, H98, and their derivatives were grown at 45°C in liquid (orbital shaker at 250 rpm, 1-in orbital diameter) or on solid agar [1.5% (wt/vol)] in either semi-defined Casamino Acid (Fisher Scientific) Hv-Cab medium (23) supplemented with uracil (50 µg mL^{-1} final concentration, Sigma) or Modified Growth Medium (MGM) (38). Hv-Cab requires further supplementation with tryptophan (50 µg mL^{-1} final, Fisher Scientific) or with thymidine (40 µg mL^{-1} final, Acros Organics) and hypoxanthine (40 µg mL^{-1} final, Sigma) for H53 and derivatives or for H98 and derivatives, respectively. MGM requires no additional supplementation. Upon transformation with plasmid constructs that encode *pyrE2* or *hdrB*, supplementation with uracil or thymidine/hypoxanthine in Hv-Cab is no longer required. Solid agar plates are placed within sealable bags during incubation to prevent the plates from drying out. *Escherichia coli* strains were grown at 37°C in NZCYM (Research Products International,RPI) medium supplemented with ampicillin (100 µg mL^{-1} final, Corning) (39).

EMS mutagenesis and motility screen

The Δ*pilA*[*1-6*] strain was inoculated in MGM and grown to stationary phase (OD_{600} 1.0). The cultures were then diluted with fresh MGM at 1:10. The sub-inoculation was then grown until OD 0.3–0.4. Two milliliters of aliquots of the culture (approx. 10^7 cells) was transferred to five microcentrifuge tubes corresponding to five experimental conditions: the negative control with no EMS exposure as well as 0, 10, 20, and 30 minutes of EMS exposure. Cells were centrifuged and washed twice with sodium chloride, magnesium sulfate, and Tris (SMT) buffer (3.5 M NaCl, 0.15 M $MgSO_4$, 10 mM Tris-Cl, and pH 7.2) and then resuspended with SMT buffer. About 10.29 µL EMS (0.05 M) was added to the tubes, mixed thoroughly, and incubated for the corresponding length of exposure time. Cells were then centrifuged and washed twice with SMT buffer. Using a toothpick, a cell pellet was touched, and stab lines were made into 0.35% agar MGM plates. Plates were incubated upright at 45°C for 3–5 days until small halos extending from the stab lines started to appear. Motility phenotype was confirmed by using a toothpick to touch the halo, re-streak onto solid agar [1.5% (wt/vol)], and re-stab single isolated colonies onto 0.35% (wt/vol) agar MGM plates.

Sequencing Δ*pilA*[*1-6*] suppressor strains

The methods for cell cultivation, DNA extraction, and sequencing were the same as described previously for mutants derived from the H295 strain (40), but here, the parent strain was the H53 strain of *H. volcanii* (Δ*pyrE2* and Δ*trpA*), which similarly has the pHV4 plasmid integrated into the chromosome and lacks pHV2. The sequence reads (Illumina,

paired-end, 150 cycle reads) for the suppressor strains were imported into Geneious Prime (v. 2023.2.1), trimmed using BBDuk (v. 38.84; default settings) from the BBTools package (41), and mapped to the genome sequence of the parental strain (H53) using the Bowtie2 mapper (v. 2.4.5). The mapped assemblies were scanned manually within Geneious in order to detect all differences across the entire genome of each strain. Mutations for each strain are listed in Table S1.

Protein amino acid sequence alignments

Protein sequences of *H. volcanii* DS2 ArlI (arCOG 01817), ArlJ (arCOG 01809), and CirA (arCOG 01171) were found on the UniProt protein database, and a protein BLAST search was performed of microbial genomes within GenBank on the NCBI website. Four haloarchaea species (*Haloarcula marismortui*, *Halobacterium jilantaiense*, *Halobacterium salinarium*, and *Natronomonas pharaonis*) and five other representative archaeal species from different phyla (*S. acidocaldarius*, *Aeropyrum pernix*, *Methanocaldococcus jannaschii*, *Methanofollis liminatans*, and *Thermococcus kodakarensis*) were chosen for the sequence alignment. Sequences were aligned via Clustal Omega Multiple Sequence Alignment (42), and the output URL was imported to Jalview (v. 2.11.3.2) (43). Aligned residues were colored on Jalview according to "Percentage Identity" and the program automatically assigned darker blue color residues to indicate a higher percentage of conservation. Residues corresponding to the point mutations of *H. volcanii* ArlI, ArlJ, and CirA from Table 1 were labeled. The conserved motifs for ArlI proteins which had previously been identified in *S. acidocaldarius* ArlI (Walker A and Walker B nucleotide binding ATPase sites, the aspartate box, and the histidine box) (29) were identified and indicated in Fig. S1. The conserved motifs for *H. volcanii* CirA (Walker A and Walker B domains, catalytic glutamate residues) (26) were identified and indicated in Fig. S1.

Protein structure prediction and modeling

The hexameric structure of the ArlI complex was predicted using a local installation of AlphaFold-Multimer (30). AlphaFold-Multimer simulations were performed on the Wistar Institute High-Performance Cluster. Five structures were predicted without a template, and the top-ranked structure in terms of ipTM + pTM score was inspected using Pymol 2.5.5. The structure of the ArlJ complex was generated using AlphaFold (v. 2.3.1) (44) via LocalColabFold (v. 1.5) (45) using the default settings. Computations were performed on the Penn Arts and Sciences General Purpose Cluster. Structure files from both ArlI and ArlJ were imported into the iCN3D web-based 3D-structure viewer (46) for visualization, color adjustments, and locating the residues of interest from Table 1. Transmembrane regions of the ArlJ dimer were determined by SignalP 6.0(32), and the orientation of the protein complex was adjusted with respect to the extracellular and cytoplasmic regions.

Plasmid preparation and *H. volcanii* transformation

The pTA131 plasmid was used to generate chromosomal deletions (47), and the pTA963 overexpression plasmid was used for complementation and *in trans* expression experiments (33). DNA Phusion-Taq polymerase, restriction enzymes, and DNA ligase were purchased from New England BioLabs. Plasmids were initially transformed into *E. coli* DH5α cells; plasmids were then transformed into *E. coli* DAM$^-$ strain DL739 prior to *H. volcanii* transformation. Plasmid preparations for both *E. coli* strains were performed using the PureLink Quick Plasmid Miniprep Kit (Invitrogen). *H. volcanii* transformations were performed using the polyethylene glycol method (38). All oligonucleotides used to construct the recombinant plasmids are listed in Table S4.

Generation of chromosomal deletions

Chromosomal deletions were generated by the homologous recombination method (pop-in/pop-out), as previously described (47). Plasmid constructs for use in the pop-in/pop-out deletion process were generated by using overlap PCR, as previously described

(48). About 750 nucleotides flanking the corresponding gene were amplified via PCR (for primers Table S4). This resulted in an overlapping region between the upstream and downstream fragments, which were subsequently fused by overlap PCR. The fused upstream and downstream fragments were then cloned into the haloarchaeal suicide vector pTA131 via digestion with XbaI and XhoI followed by ligation (47). For the *cirA* deletion construct, XbaI and HindIII were used because *cirA* has an internal XhoI site. The resulting constructs were verified by Sanger sequencing. The knockout plasmid constructs for Δ*arlI*, Δ*arlJ*, and Δ*cirA* were transformed into H53 wild type to generate the single deletion strains. Additionally, the plasmid constructs for Δ*arlI* and Δ*arlJ* were transformed into the Δ*pilA[1-6]* background (27) to generate multi-deletion strains. Pop-out transformants were selected on agar plates containing 5-fluoroorotic acid (Toronto Research Chemicals Inc.) at a final concentration of 50 µg mL^{-1}. Successful gene deletion was confirmed by PCR using primers within the deleted gene as well as the upstream and downstream primers used for initial plasmid construction. Deletion strains were further analyzed by Illumina whole-genome sequencing and variant calling performed by SeqCenter (Pittsburgh, PA, USA) to confirm the complete deletion of the gene as well as search for any secondary genome alteration. Ilumina sequencing libraries were prepared using the tagmentation-based Illumina DNA Prep kit and custom Integrated DNA Technologies (IDT) 10 bp unique dual indices with a target insert size of 280 bp. No additional DNA fragmentation or size selection steps were performed. Illumina sequencing was performed on an Illumina NovaSeq X Plus sequencer, producing 2 × 150 bp paired-end reads. Demultiplexing, quality control, and adapter trimming were performed with bcl-convert1 (v4.2.4). Variant calling was carried out using BreSeq (v0.38.1) under default settings using *H. volcanii* DS2 (GCF_000025685.1) as a reference.

Construction of expression plasmids

For gene complementation studies, *in trans* expression of *arlI*, *arlJ*, or *cirA* was performed using pTA963, which includes a tryptophan-inducible promoter (p.*tna*) for the inserted genes (33). The primers to amplify out the respective gene are listed in Table S4. The reverse primers were designed to incorporate a 6xHis-Tag to the end of the gene to enable the expression of proteins for downstream protein purification applications. For *arlI* and *arlJ*, the PCR-amplified genes were ligated into pTA963; both the vector and the amplified gene fragment were digested with BamHI and EcoRI prior to ligation. The resulting constructs were verified by Sanger sequencing. For complementation, deletion strains were transformed with the plasmid containing the corresponding gene or with empty vector pTA963 as a control.

Motility plate assay

Motility assays were assessed on 0.35% (wt/vol) agar Hv-Cab medium with supplements as required. A toothpick was used to stab-inoculate the agar followed by incubation at 45°C upright in a plastic box with added wet paper towels to maintain humidity. Paper towels were changed daily. Motility assay plates were removed from the 45°C incubator after 3 days and imaged after 1 day of room temperature incubation as this increased the carotenoid production, allowing for better visibility of the halos. Motility halos were quantified using Fiji (ImageJ; v. 2.9.0) (49). Images were uploaded to Fiji, and the scale was set based on plate diameter. Statistical significance of halo diameters was assessed with an unpaired *t* test using GraphPad Prism v. 9.5.1 (528) for macOS (GraphPad Software, San Diego, CA, USA, www.graphpad.com).

Cell pellets

Liquid cultures in Hv-Cab medium with supplements as required of *H. volcanii* wild type and Δ*cirA* were grown until OD_{600} 0.55. One milliliter of each culture was centrifuged in 1.5 mL Eppendorf tubes at 4,900 × *g* for 6 minutes, and the supernatant was aspirated out. The resulting pellets were imaged.

Growth curve

Growth curves for H53 wild type and Δ*cirA* strains were measured using BioTek Epoch 2 microplate reader with BioTek Gen6 v.1.03.01 (Agilent). Colonies of each strain were inoculated in 5 mL Hv-Cab liquid medium and grown shaking at 45°C until an OD_{600} 0.15 was reached. Cultures were diluted to an OD_{600} 0.01 with fresh liquid medium in a final volume of 200 µL in each well of a non-treated and flat-bottom polystyrene 96-well plate (Corning). Eight biological replicates were used for each strain. To help prevent evaporation, two rows of perimeter wells were aliquoted with 200 µL of media, and a two-degree gradient was specified in the 45°C temperature setting. Readings were taken every 30 minutes with double orbital, continuous fast shaking (335 cpm, 4 mm) in between. Readings were taken at a wavelength of 600 nm for a total of 48 hours and then plotted in GraphPad Prism v. 9.5.1 (528) for macOS (GraphPad Software, San Diego, CA, USA, www.graphpad.com).

CFU counting

5 mL liquid cultures of the H53 wild type and Δ*cirA* strains was inoculated in liquid Hv-Cab medium and grown to OD_{600} 0.5. 30 µL of a 10^{-5} dilution was spread onto Hv-Cab solid agar plates in three technical replicates and incubated for 5 days. Images were taken, and CFUs were counted using the Fiji (ImageJ; v. 2.9.0) "Cell Counter" feature (49). Statistical significance was analyzed with an unpaired *t* test using GraphPad Prism v. 9.5.1 (528) for macOS (GraphPad Software, San Diego, CA, USA, www.graphpad.com).

Cell shape imaging

5 mL of liquid cultures of the H53 wild type and Δ*cirA* strains was inoculated and incubated, with shaking, at 45°C until OD_{600} 0.05 and 0.35 were reached, corresponding to early- and mid-log growth phase, respectively. One milliliter from each culture was centrifuged at 4,900 × g for 6 minutes. The supernatant was aspirated to leave ~5 µL liquid remaining with the pellet for the cultures at OD_{600} 0.05 (200 times concentrated) and ~100 µL liquid remaining with the pellet for the cultures at OD_{600} 0.35 (10 times concentrated). Pellets were resuspended in the corresponding remaining liquid, 1.5 µL of resuspension was placed on glass slides (Fisher Scientific), and a glass coverslip (Globe Scientific Inc.) was placed on top. Slides were visualized using a Leica Dmi8 inverted microscope attached to a Leica DFC9000 GT camera with Leica Application Suite X (v. 3.6.0.20104) software. Differential interference contrast images were captured at 100× magnification.

Quantitative RT-PCR

5 mL liquid cultures of H53 wild type and Δ*cirA* strains were inoculated and incubated, shaking, at 45°C until OD_{600} 0.05 and 0.35 were reached, corresponding to early and mid-log growth phase, respectively. Four milliliters of the early-log cultures and 0.5 mL of the mid-log cultures were harvested and pelleted at 4,900 × *g* for 6 minutes. RNA was extracted using the Qiagen RNeasy Plus Micro Kit and lysate homogenized with Qiagen QIAshredder columns. RNA concentration was determined with Qubit RNA High Sensitivity Assay Kits. Two micrograms of RNA from each condition was treated with 2 units of Promega RQ1 RNase-free DNase, incubated at 37°C for 45 minutes, and then DNase was heat inactivated. cDNA was synthesized from RNA using ProtoScript II First Strand cDNA Synthesis Kit (New England BioLabs) using random primers (included with kit). PrimeTime qPCR Primers for *H. volcanii arlA1*, *arlI*, *arlJ*, and 16S rRNA were designed using IDT (Table S4). qRT-PCR reaction mixtures were set up with 10 µL of SYBR Green JumpStart *Taq* ReadyMix (Sigma-Aldrich), 2 µL primers (final concentration 1 µM), 1 µL of cDNA from each experimental condition, and nuclease-free water for a total reaction volume of 20 µL. Each reaction was performed with five technical replicates on QuantStudio 3 Real-Time PCR System using the $\Delta\Delta C_t$ experiment type. The thermal cycling conditions were as follows: initial denaturation 94°C for 2 minutes, then 40 cycles

of 94°C for 15 s and 60°C for 1 minute. The SYBR Green fluorescence signal was recorded at the end of each cycle, and the cycle threshold (C_t) was automatically determined by the instrument. Differential expression was calculated from the negative difference in threshold crossing point ($-\Delta C_t$) between the primers of interest (targeting *arlA1*, *arlI*, *arlJ*) and control primers that target 16S rRNA. $-\Delta C_t$ values were plotted in GraphPad Prism v. 9.5.1 (528) for macOS (GraphPad Software, San Diego, CA, USA, www.graphpad.com).

ACKNOWLEDGMENTS

We gratefully acknowledge Wil Prall for his assistance with the qRT-PCR data analysis. We also thank Dr. Alex Bisson, Dr. Friedhelm Pfeiffer, and Yirui Hong for their insightful comments on this manuscript.

This work was supported by National Science Foundation grant NSF-MBC2222076 and a University of Pennsylvania Research Fund grant. P.C. was additionally supported by a National Institutes of Health Training Grant T32 GM007229 "Cell and Molecular Biology." M.A.G. was supported by a Merck/PennFERBS fellowship.

AUTHOR AFFILIATIONS

[1]Department of Biology, University of Pennsylvania, Philadelphia, Pennsylvania, USA
[2]Department of Microbiology, Perelman School of Medicine, University of Pennsylvania, Philadelphia, Pennsylvania, USA
[3]Vaccine and Immunotherapy Center, The Wistar Institute, Philadelphia, Pennsylvania, USA
[4]Computational Biology Group, Max Planck Institute of Biochemistry, Martinsried, Germany
[5]Veterinary Biosciences, Faculty of Veterinary and Agricultural Sciences, University of Melbourne, Parkville, Australia

PRESENT ADDRESS

Kun Yun, Mayo Clinic Graduate School of Biomedical Sciences, Rochester, Minnesota, USA
Georgio P. Legerme, Department of Psychiatry, University of Florida College of Medicine, Gainesville, Florida, USA
Manuela Tripepi, Department of Biology, Thomas Jefferson University, Philadelphia, Pennsylvania, USA
Criston Young, Department of Ophthalmology, Scheie Eye Institute Penn Presbyterian, Philadelphia, Pennsylvania, USA

AUTHOR ORCIDs

Priyanka Chatterjee http://orcid.org/0000-0003-1608-7190
Manuela Tripepi http://orcid.org/0000-0002-1275-7380
Daniel Kulp http://orcid.org/0000-0002-0527-3804
Mike Dyall-Smith http://orcid.org/0000-0002-1880-1960
Mecky Pohlschroder http://orcid.org/0000-0001-7729-1342

FUNDING

Funder	Grant(s)	Author(s)
National Science Foundation (NSF)	NSF-MBC2222076	Mecky Pohlschroder
HHS | National Institutes of Health (NIH)	T32 GM007229	Priyanka Chatterjee

AUTHOR CONTRIBUTIONS

Priyanka Chatterjee, Conceptualization, Data curation, Formal analysis, Investigation, Methodology, Visualization, Writing – original draft, Writing – review and editing | Marco A. Garcia, Conceptualization, Investigation, Visualization, Writing – original draft | Jacob A. Cote, Formal analysis, Writing – review and editing | Kun Yun, Investigation | Georgio P. Legerme, Methodology | Rumi Habib, Formal analysis, Investigation, Writing – original draft | Manuela Tripepi, Resources | Criston Young, Resources | Daniel Kulp, Supervision | Mike Dyall-Smith, Data curation, Formal analysis, Writing – original draft | Mecky Pohlschroder, Conceptualization, Formal analysis, Funding acquisition, Project administration, Supervision, Visualization, Writing – original draft, Writing – review and editing

DATA AVAILABILITY

Raw sequencing results for WGS of the Δ*pilA*[*1-6*] suppressor strains and raw values for the growth curve and qRT-PCR can be found at 10.5281/zenodo.10735612. All other data types associated with this article can be found in the supplemental material.

ADDITIONAL FILES

The following material is available online.

Supplemental Material

Supplemental figures (JB00089-24-s0001.docx). Figures S1 to S3; legends for Tables S1 to S4.
Supplemental tables (JB00089-24-s0002.xlsx). Tables S1 to S4.

REFERENCES

1. Keegstra JM, Carrara F, Stocker R. 2022. The ecological roles of bacterial chemotaxis. Nat Rev Microbiol 20:491–504. https://doi.org/10.1038/s41579-022-00709-w
2. Szurmant H, Ordal GW. 2004. Diversity in chemotaxis mechanisms among the bacteria and archaea. Microbiol Mol Biol Rev 68:301–319. https://doi.org/10.1128/MMBR.68.2.301-319.2004
3. Khan S, Scholey JM. 2018. Assembly, functions and evolution of archaella, flagella and cilia. Curr Biol 28:R278–R292. https://doi.org/10.1016/j.cub.2018.01.085
4. Beeby M, Ferreira JL, Tripp P, Albers S-V, Mitchell DR. 2020. Propulsive nanomachines: the convergent evolution of archaella, flagella and cilia. FEMS Microbiol Rev 44:253–304. https://doi.org/10.1093/femsre/fuaa006
5. Jarrell KF, Albers S-V, Machado J de S. 2021. A comprehensive history of motility and archaellation in archaea. FEMS Microbes 2:xtab002. https://doi.org/10.1093/femsmc/xtab002
6. Craig L, Pique ME, Tainer JA. 2004. Type IV pilus structure and bacterial pathogenicity. 5. Nat Rev Microbiol 2:363–378. https://doi.org/10.1038/nrmicro885
7. Trachtenberg S, Cohen-Krausz S. 2006. The archaeabacterial flagellar filament: a bacterial propeller with a pilus-like structure. J Mol Microbiol Biotechnol 11:208–220. https://doi.org/10.1159/000094055
8. Szabó Z, Stahl AO, Albers S-V, Kissinger JC, Driessen AJM, Pohlschröder M. 2007. Identification of diverse archaeal proteins with class III signal peptides cleaved by distinct archaeal prepilin peptidases. J Bacteriol 189:772–778. https://doi.org/10.1128/JB.01547-06
9. Pohlschroder M, Ghosh A, Tripepi M, Albers S-V. 2011. Archaeal type IV pilus-like structures—evolutionarily conserved prokaryotic surface organelles. Curr Opin Microbiol 14:357–363. https://doi.org/10.1016/j.mib.2011.03.002
10. Pohlschroder M, Esquivel RN. 2015. Archaeal type IV pili and their involvement in biofilm formation. Front Microbiol 6:190. https://doi.org/10.3389/fmicb.2015.00190
11. Ghosh A, Albers SV. 2011. Assembly and function of the archaeal flagellum. Biochem Soc Trans 39:64–69. https://doi.org/10.1042/BST0390064
12. Pohlschroder M, Pfeiffer F, Schulze S, Abdul Halim MF. 2018. Archaeal cell surface biogenesis. FEMS Microbiol Rev 42:694–717. https://doi.org/10.1093/femsre/fuy027
13. Nuno de Sousa Machado J, Albers S-V, Daum B. 2022. Towards elucidating the rotary mechanism of the archaellum machinery. Front Microbiol 13:848597. https://doi.org/10.3389/fmicb.2022.848597
14. Chaudhury P, van der Does C, Albers S-V. 2018. Characterization of the ATPase FlaI of the motor complex of the *Pyrococcus furiosus* archaellum and its interactions between the ATP-binding protein FlaH. PeerJ 6:e4984. https://doi.org/10.7717/peerj.4984
15. Banerjee A, Tsai C-L, Chaudhury P, Tripp P, Arvai AS, Ishida JP, Tainer JA, Albers S-V. 2015. FlaF is a β-sandwich protein that anchors the archaellum in the archaeal cell envelope by binding the S-layer protein. Structure 23:863–872. https://doi.org/10.1016/j.str.2015.03.001
16. Tsai C-L, Tripp P, Sivabalasarma S, Zhang C, Rodriguez-Franco M, Wipfler RL, Chaudhury P, Banerjee A, Beeby M, Whitaker RJ, Tainer JA, Albers S-V. 2020. The structure of the periplasmic FlaG–FlaF complex and its essential role for archaellar swimming motility. Nat Microbiol 5:216–225. https://doi.org/10.1038/s41564-019-0622-3
17. Göker M, Oren A. 2023. Valid publication of four additional phylum names. Int J Syst Evol Microbiol 73:006024. https://doi.org/10.1099/ijsem.0.006024
18. Makarova KS, Koonin EV, Albers S-V. 2016. Diversity and evolution of type IV pili systems in archaea. Front Microbiol 7:667. https://doi.org/10.3389/fmicb.2016.00667
19. Arahal DR, Bull CT, Christensen H, Chuvochina M, Dedysh SN, Fournier P-E, Konstantinidis KT, Parker CT, Ventosa A, Young P, Göker M. 2024. Judicial opinion 129. Int J Syst Evol Microbiol 74:006064. https://doi.org/10.1099/ijsem.0.006064
20. Chaudhury P, Neiner T, D'Imprima E, Banerjee A, Reindl S, Ghosh A, Arvai AS, Mills DJ, van der Does C, Tainer JA, Vonck J, Albers S-V. 2016. The

nucleotide-dependent interaction of FlaH and FlaI is essential for assembly and function of the archaellum motor. Mol Microbiol 99:674–685. https://doi.org/10.1111/mmi.13260
21. de Sousa Machado JN, Vollmar L, Schimpf J, Chaudhury P, Kumariya R, van der Does C, Hugel T, Albers S-V. 2021. Autophosphorylation of the KaiC-like protein ArLH inhibits oligomerization and interaction with ArlI, the motor ATPase of the archaellum. Mol Microbiol 116:943–956. https://doi.org/10.1111/mmi.14781
22. Makarova KS, Galperin MY, Koonin EV. 2017. Proposed role for KaiC-like ATPases as major signal transduction hubs in archaea. mBio 8:e01959-17. https://doi.org/10.1128/mBio.01959-17
23. de Silva RT, Abdul-Halim MF, Pittrich DA, Brown HJ, Pohlschroder M, Duggin IG. 2021. Improved growth and morphological plasticity of *Haloferax volcanii*. Microbiology (Reading) 167:001012. https://doi.org/10.1099/mic.0.001012
24. Duggin IG, Aylett CHS, Walsh JC, Michie KA, Wang Q, Turnbull L, Dawson EM, Harry EJ, Whitchurch CB, Amos LA, Löwe J. 2015. CetZ tubulin-like proteins control archaeal cell shape. Nature 519:362–365. https://doi.org/10.1038/nature13983
25. Schiller H, Hong Y, Kouassi J, Rados T, Kwak J, DiLucido A, Safer D, Marchfelder A, Pfeiffer F, Bisson A, Schulze S, Pohlschroder M. 2024. Identification of structural and regulatory cell-shape determinants in *Haloferax volcanii*. Nat Commun 15:1414. https://doi.org/10.1038/s41467-024-45196-0
26. Maniscalco M, Nannen J, Sodi V, Silver G, Lowrey PL, Bidle KA. 2014. Light-dependent expression of four cryptic archaeal circadian gene homologs. Front Microbiol 5:79. https://doi.org/10.3389/fmicb.2014.00079
27. Esquivel RN, Pohlschroder M. 2014. A conserved type IV pilin signal peptide H-domain is critical for the post-translational regulation of flagella-dependent motility. Mol Microbiol 93:494–504. https://doi.org/10.1111/mmi.12673
28. Paetzel M, Karla A, Strynadka NCJ, Dalbey RE. 2002. Signal peptidases. Chem Rev 102:4549–4580. https://doi.org/10.1021/cr010166y
29. Ghosh A, Hartung S, van der Does C, Tainer JA, Albers S-V. 2011. Archaeal flagellar ATPase motor shows ATP-dependent hexameric assembly and activity stimulation by specific lipid binding. Biochem J 437:43–52. https://doi.org/10.1042/BJ20110410
30. Evans R, O'Neill M, Pritzel A, Antropova N, Senior A, Green T, Žídek A, Bates R, Blackwell S, Yim J, Ronneberger O, Bodenstein S, Zielinski M, Bridgland A, Potapenko A, Cowie A, Tunyasuvunakool K, Jain R, Clancy E, Kohli P, Jumper J, Hassabis D. 2022. Protein complex prediction with AlphaFold-multimer. bioRxiv. https://doi.org/10.1101/2021.10.04.463034
31. Reindl S, Ghosh A, Williams GJ, Lassak K, Neiner T, Henche A-L, Albers S-V, Tainer JA. 2013. Insights into FlaI functions in archaeal motor assembly and motility from structures, conformations, and genetics. Mol Cell 49:1069–1082. https://doi.org/10.1016/j.molcel.2013.01.014
32. Teufel F, Almagro Armenteros JJ, Johansen AR, Gíslason MH, Pihl SI, Tsirigos KD, Winther O, Brunak S, von Heijne G, Nielsen H. 2022. SignaLP 6.0 predicts all five types of signal peptides using protein language models. Nat Biotechnol 40:1023–1025. https://doi.org/10.1038/s41587-021-01156-3
33. Allers T, Barak S, Liddell S, Wardell K, Mevarech M. 2010. Improved strains and plasmid vectors for conditional overexpression of his-tagged proteins in *Haloferax volcanii*. Appl Environ Microbiol 76:1759–1769. https://doi.org/10.1128/AEM.02670-09
34. Schulze S, Adams Z, Cerletti M, De Castro R, Ferreira-Cerca S, Fufezan C, Giménez MI, Hippler M, Jevtic Z, Knüppel R, Legerme G, Lenz C, Marchfelder A, Maupin-Furlow J, Paggi RA, Pfeiffer F, Poetsch A, Urlaub H, Pohlschroder M. 2020. The archaeal proteome project advances knowledge about archaeal cell biology through comprehensive proteomics. Nat Commun 11:3145. https://doi.org/10.1038/s41467-020-16784-7
35. Onga EA, Vêncio RZN, Koide T. 2022. Low salt influences archaellum-based motility, glycerol metabolism and gas vesicles biogenesis in *Halobacterium salinarum*. Microorganisms 10:2442. https://doi.org/10.3390/microorganisms10122442
36. Odermatt PD, Nussbaum P, Monnappa S, Talà L, Li Z, Sivabalasarma S, Albers S-V, Persat A. 2023. Archaeal type IV pili stabilize *Haloferax volcanii* biofilms in flow. Curr Biol 33:3265–3271. https://doi.org/10.1016/j.cub.2023.06.055
37. Hayashi F, Suzuki H, Iwase R, Uzumaki T, Miyake A, Shen J-R, Imada K, Furukawa Y, Yonekura K, Namba K, Ishiura M. 2003. ATP-induced hexameric ring structure of the cyanobacterial circadian clock protein KaiC. Genes Cells 8:287–296. https://doi.org/10.1046/j.1365-2443.2003.00633.x
38. Dyall-Smith M, Holmes M, Kamekura M, Lam W, Nuttall S, Woods W, Jablonski P, Serrano J, Ngui K, Antón J, et al. 2009. The halohandbook: protocols for haloarchaeal genetics
39. Caccamo PD, Brun YV. 2018. The molecular basis of noncanonical bacterial morphology. Trends Microbiol 26:191–208. https://doi.org/10.1016/j.tim.2017.09.012
40. Collins M, Afolayan S, Igiraneza AB, Schiller H, Krespan E, Beiting DP, Dyall-Smith M, Pfeiffer F, Pohlschroder M. 2020. Mutations affecting HVO_1357 or HVO_2248 cause hypermotility in *Haloferax volcanii*, suggesting roles in motility regulation. Genes (Basel) 12:58. https://doi.org/10.3390/genes12010058
41. BBMap. Sourceforge. 2023. Available from: https://sourceforge.net/projects/bbmap. Retrieved 6 Feb 2024.
42. Madeira F, Pearce M, Tivey ARN, Basutkar P, Lee J, Edbali O, Madhusoodanan N, Kolesnikov A, Lopez R. 2022. Search and sequence analysis tools services from EMBL-EBI in 2022. Nucleic Acids Res 50:W276–W279. https://doi.org/10.1093/nar/gkac240
43. Waterhouse AM, Procter JB, Martin DMA, Clamp M, Barton GJ. 2009. Jalview version 2—a multiple sequence alignment editor and analysis workbench. Bioinformatics 25:1189–1191. https://doi.org/10.1093/bioinformatics/btp033
44. Jumper J, Evans R, Pritzel A, Green T, Figurnov M, Ronneberger O, Tunyasuvunakool K, Bates R, Žídek A, Potapenko A, et al. 2021. Highly accurate protein structure prediction with AlphaFold. Nature 596:583–589. https://doi.org/10.1038/s41586-021-03819-2
45. Mirdita M, Schütze K, Moriwaki Y, Heo L, Ovchinnikov S, Steinegger M. 2022. ColabFold: Making protein folding accessible to all. Nat Methods 19:679–682. https://doi.org/10.1038/s41592-022-01488-1
46. Wang J, Youkharibache P, Zhang D, Lanczycki CJ, Geer RC, Madej T, Phan L, Ward M, Lu S, Marchler GH, Wang Y, Bryant SH, Geer LY, Marchler-Bauer A. 2020. iCn3D, a web-based 3D viewer for sharing 1D/2D/3D representations of biomolecular structures. Bioinformatics 36:131–135. https://doi.org/10.1093/bioinformatics/btz502
47. Allers T, Ngo HP, Mevarech M, Lloyd RG. 2004. Development of additional selectable markers for the halophilic archaeon *Haloferax volcanii* based on the *leuB* and *trpA* genes. Appl Environ Microbiol 70:943–953. https://doi.org/10.1128/AEM.70.2.943-953.2004
48. Tripepi M, Imam S, Pohlschröder M. 2010. *Haloferax volcanii* flagella are required for motility but are not involved in PibD-dependent surface adhesion. J Bacteriol 192:3093–3102. https://doi.org/10.1128/JB.00133-10
49. Schindelin J, Arganda-Carreras I, Frise E, Kaynig V, Longair M, Pietzsch T, Preibisch S, Rueden C, Saalfeld S, Schmid B, Tinevez J-Y, White DJ, Hartenstein V, Eliceiri K, Tomancak P, Cardona A. 2012. Fiji: an open-source platform for biological-image analysis. Nat Methods 9:676–682. https://doi.org/10.1038/nmeth.2019